Full Paper Wiley Online Library ELECTROANALYSIS

DOI: 10.1002/elan.201500009

Sensitivity Enhancement in Nickel Hydroxide/3D-Graphene as Enzymeless Glucose Detection

Iman Shackery,[a] Umarkant Patil,[a] Min-Jung Song,[b] Ji Soo Sohn,[a] Sachin Kulkarni,[a] Surajit Some,[c] Su Chan Lee,[a] Min Sik Nam,[a] Wooyoung Lee,[d] and Seong Chan Jun*[a]

Abstract: A nickel hydroxide ($Ni(OH)_2$)/3D-graphene composite is used as monolithic free-standing electrode for enzymeless electrochemical detection of glucose. $Ni(OH)_2$ nanoflakes are synthesized by using a simple solution growth procedure on 3D-graphene foam which was grown by chemical vapor deposition (CVD). The pore structure of 3D-graphene allows easy access to glucose with high surface area, which leads to glucose detection with an ultrahigh sensitivity of 3.49 $mA\,mM^{-1}\,cm^{-2}$ and a significant lower detection limit up to 24 nM. Cyclic voltammetry (CV) and potentionstatic mode is used for non-enzymatic glucose sensing. The impedance and effective surface area have been studied well. The high sensitivity, low detection limit and simple configuration of $Ni(OH)_2$/three dimensional (3D)-graphene composite electrodes can evoke its industrial application in glucose sensing devices.

Keywords: 3D-graphene · Nickel hydroxide · Nanoflakes · Enzymeless glucose sensing

1 Introduction

Glucose sensing has been widely implemented in clinical analysis and biotechnology for early detection or diagnosis of diabetes. Although the glucose sensing for the blood sugar determination is the most important application of glucose detection, the development of suitable chemical sensors for monitoring the glucose in food and drink products and technological processes, are also being actively pursued by academic and industrial researchers. Usually, glucose biosensors are based on glucose oxidase with their high selectivity [1]. In order to gain excellent sensitivity and high selectivity of the blood sugar meter, enzymatic glucose sensors, such as oxygen-mediated electrode, artificial mediator type, and direct electron transfer type, have been widely developed [2]. However, some drawbacks of enzymatic sensors are also founded in glucose oxidase-based biosensors such as it is too sensitive to the thermal and chemical conditions [1c,3]. These disadvantages of enzymatic sensors that is originated from the nature of enzymes, limit the application of glucose biosensors greatly.

Many attempts have been made to develop glucose sensors without glucose oxidase to solve these problems. Nonenzymatic glucose sensors have many advantages, such as simplicity and good stability. Numerous nanostructured materials have been applied to develop innovative nonenzymatic glucose sensors due to their catalysis to the oxidation of glucose. In recent years the nonenzymatic glucose sensors based on metal oxides and metal hydroxide attract great interest due to fast response, high sensitivity, low detection limit, good stability and low cost. We can mention metal oxide such as Cu_xO [4], NiO [5], MnO_2 [6], Co_3O_4 [7] etc. and metal hydroxide such as $Ni(OH)_2$ [8], $Cu(OH)_2$ [9], $Co(OH)_2$ [10] etc. Among all nonenzymatic glucose sensors, the $Ni(OH)_2$-based sensors have excellent electro-catalysis toward glucose [8,11], ascribing to the redox pair of $Ni(OH)_2$/NiOOH in which NiOOH can be deoxidized by glucose easily [8a,12]. Despite all the advantages of metal oxides/hydroxides as glucose sensor, its resistivity restricts the sensing performance. Therefore, the development of nonenzymatic glucose sensors with low cost, high selectivity and quick response is still challenging.

To detect Glucose and see whether individual substance can detect glucose or not there are several methods such as radio frequency (RF) technique, cyclic voltammetry (CV), chronoamperometric and so on [13].

[a] I. Shackery,[#] U. Patil,[#] J. S. Sohn, S. Kulkarni, S. C. Lee, M. S. Nam, S. C. Jun
School of Mechanical Engineering, Yonsei University
Seoul 120–749, Republic of Korea
*e-mail: scj@yonsei.ac.kr

[b] M.-J. Song[#]
College of Liberal Art & Interdisciplinary Studies, Kyonggi University
Yeongtong-gu, Suwon-si, Gyeonggi-do 443-760, Republic of Korea

[c] S. Some
Department of Dyestuff Technology, Institute of Chemical Technology
Matunga, Mumbai-400 019, India

[d] W. Lee
Department of Materials Science and Engineering, Yonsei University
Seoul 120–749, Republic of Korea

[#] These authors contributed equally to this work.

Supporting information for this article is available on the WWW under http://dx.doi.org/10.1002/elan.201500009.

Graphene, a two-dimensional monolayer of sp^2-hybridized carbon atoms, has attracted enormous interest in recent years due to its extraordinary unusual mechanical strength, chemical stability, high electrical conductivity (103–104 $S\,m^{-1}$) [14], and ultra large specific surface area (~2600 $m^2\,g^{-1}$ for single-layer graphene) [15].These unique characteristics hold great promise for potential applications in many technological fields. Especially graphene can play an important part in improving the performance of sensors due to their large specific surface area and excellent electrical conductivity [4,16]. Consequently, many approaches have been explored to fabricate graphene-based nano-composites for biosensors [7b,17]. Among all of them, a lightweight 3D-graphene foam (low density of ~20 $mg\,cm^{-3}$), attains great attraction in supercapacitors and glucose sensors, because of its unique properties like lightweight and continuous 3D conducting porous structure. The integration of various 3D-macroporous structures of graphene fused with numerous materials has been extensively used to grow more conductive, porous, and flexible films with a higher stiffness and strength to broaden their application area [7b,18]. In present manuscript, a nonenzymatic glucose sensor based on a $Ni(OH)_2$/3D-graphene was fabricated by a simple solution growth procedure, serving as a free-standing monolithic electrode, it demonstrates better sensitivity compare to previous report [19]. The effective surface area, reproducibility and electrochemical impedance spectroscopy (EIS) of $Ni(OH)_2$/3D-graphene in presence of glucose is studied for the first time.

2 Experimental

2.1 Growth of 3D-Graphene Networks by Chemical Vapor Deposition

The 3D-graphene framework is synthesized by CVD method, using nickel foam as a template [18]. For further explanation see Supporting Information (SI).

2.2 Preparation of $Ni(OH)_2$ Nanoflakes on 3D-Graphene

The $Ni(OH)_2$ microflakes were prepared by mixing 0.1 M Nickel(II) chloride hexahydrate (Sigma-Aldrich USA) and 0.1 M urea ($CO(NH_2)_2$) as an oxidant (Sigma-Aldrich USA) in 50 mL of DI water. The 3D skeleton of graphene was dipped in a prepared bath with the support of glass micro slides. Then, the prepared bath was heated at 90 °C for 6 up to 10 hours (see Table S2 Supporting Information). After cooling to room temperature, the graphene foams with $Ni(OH)_2$ deposits were washed with deionized (DI) water and dried at room temperature.

2.3 Glucose Solution

To prepare Glucose solution, first we make Phosphate buffered saline (PBS) tablet (invitrogen) and dissolve in 100 mL Distilled water (DI). Then 0.006 g Glucose (Sigma-Aldrich) was added to achieve 0.33 mM of glucose. At the next step 50 μL of this solution add in 18 mL of PBS solution. Finally 0.92 μM of Glucose achieved.

2.4 Characterization

The electrode materials were structurally characterized by Raman, XRD, FESEM, and XPS measurements. Raman spectra were recorded at ambient temperature on a WITeck ALPHA300 M Raman System (excitation at 532 nm, 2.33 eV). The X-ray diffraction (XRD) was carried out on a Rigaku Ultima diffractometer using Cu-Kα radiation. The morphology of the composite was examined by field effect scanning electron microscopy (FESEM), (JSM-7001F, JEOL). X-ray photoelectron spectroscopy (XPS) measurements were carried out on a thermo scientific ESCALAB 250 (Thermo Fisher Scientific, UK).

2.5 Electrochemical Measurements

The $Ni(OH)_2$ grown on 3D-graphene was used as a working electrode in a three-electrode system. All of the electrochemical measurements were performed in a conventional three-electrode system with Ag/AgCl as a reference electrode and platinum (Pt) as the counter electrode in a 1 M KOH aqueous solution as the electrolyte. To carry out effective surface area the experiment was done in a 3 M KCl solution harboring 10 mM potassium ferricyanide. The three-electrode system was used to evaluate the individual performances of each electrode. All electrochemical measurements were carried out on the aforementioned workstation with the same three-electrode configuration at room temperature (25 ± 3 °C).

3 Results and Discussion

3.1 Film Formation and Reaction Mechanism

The black colored 3D porous graphene foam was prepared by CVD method, digital photograph of graphene foam is shown in the Figure 1. The Raman spectra of 3D-graphene at different places on the foam exhibited two distinct peaks at ~1559 cm^{-1} (G-band) and 2699 cm^{-1} (2D-band), confirms the formation of multilayered graphene foam, which is shown in figure S1 (see supporting information).

Synthesis of $Ni(OH)_2$ on graphene foam was achieved by using the solution growth method. The solution growth method is one of the efficient "bottom-up" approaches to grow metal hydroxide; it is based on the formation of a solid phase from solution, which involves three collective steps: nucleation, coalescence and particle growth. Detail growth mechanism of $Ni(OH)_2$ flakes on graphene foam is shown in Figure 1. The crystal formation process of the precursor can be classified as heterogeneous nucleation and subsequent crystal growth. If only crystal seeds are produced on the heterogeneous

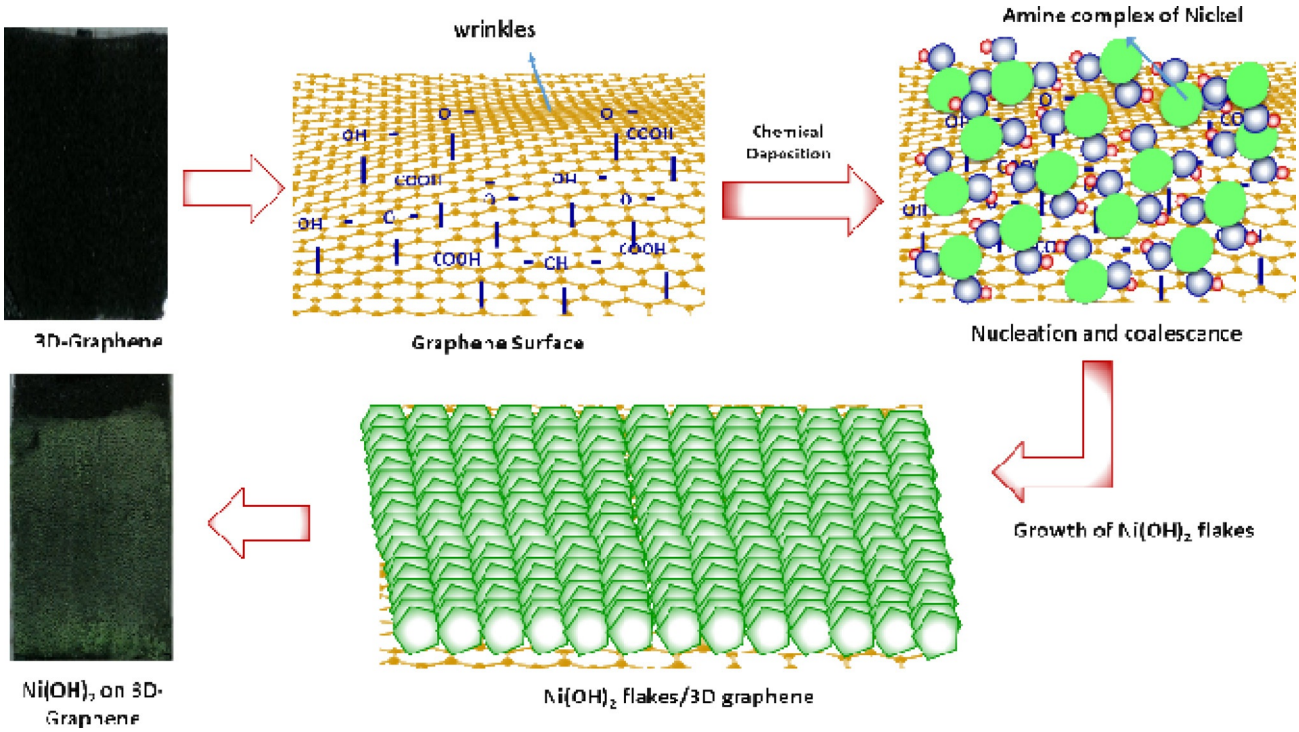

Fig. 1. Schematic of growth mechanism for formation of $Ni(OH)_2$ flakes on graphene foam. Digital photograph of graphene foam and growth mechanism of $Ni(OH)_2$ shown in figure. Formation of $Ni(OH)_2$ on graphene foam involves three collective steps: nucleation, coalescence and particle growth.

substrate, the subsequent growth of a porous film will be feasible. During the preparation of graphene on Ni foam by the CVD method, the mechanism allows the formation of some wrinkles on the surface of the graphene skeleton due to grain boundaries of Ni. Carboxyl, hydroxyl and epoxy groups were obtained on the graphene surface during Ni foam etching. Such wrinkles, carboxyl, hydroxyl and epoxy groups on the graphene skeleton are favorable for the nucleation of crystal seeds. In the formation $Ni(OH)_2$ flakes, as the temperature of solution bath increased to 120 °C, decomposition of urea (Reaction 1) took place, producing CO_2 and NH_3 gradually [20]:

$$NH_2CONH_2 + H_2O \xrightarrow{\Delta} 2NH_3 + CO_2 \quad (1)$$

After decomposition of urea, as per the above reaction, the solution became alkaline; such an alkaline condition is more favorable to generate more carboxyl, hydroxyl and an epoxy group on graphene surface. Increased carboxyl, hydroxyl and epoxy groups are constructed in order to create more nucleation sites (Figure 1).

Simultaneously, Ni^{2+} from $NiCl_2$ get mixed with NH_3, which formed amine complex. Such amine complexed metal ions easily get adsorbed on the heterogeneous surface of the substrate by electrostatic or van der Waals force (figure 1). The high specific surface area of graphene foam makes it easy to adsorb a large number of amine complexed Ni^{2+} [20]:

$$Ni^{2+} + NH_3 \rightarrow Ni(NH_3)_4{}^{2+} \quad (2)$$

Initially, the solution was neutral with pH about 6–7 and then increased gradually and monotonically with time and temperature, the solution became alkalescent. At this alkalescent bath condition, the $Ni(NH_3)_4^{2+}$is instable and the following reaction occur to form mixed metal hydroxides on the graphene surface in form of nano flakes [20]

$$Ni(NH_3)_4{}^{2+} + 2OH^- \rightarrow Ni(OH)_2 + 4\ NH_3 \quad (3)$$

In the film formation, the NH_3 released from urea was introduced as a complexing agent in the bath and exerted itself to control the release velocity of Ni^{2+} ions for deposition of the $Ni(OH)_2$ flakes. According to the above growth mechanism, the growth of green colored $Ni(OH)_2$ fastened on graphene foam surface and its digital photograph is shown in Figure 1.

3.2 Structural Studies

Film crystallinity was analyzed using X-ray diffraction. The XRD patterns of $Ni(OH)_2$ films on graphene foam are shown in Figure 2. The strong diffraction peaks at 2θ of 26.4° and 54.5° in all patterns are attributed to the (002) and (004) reflections of the crystalline peaks of hexagonal graphite carbon, marked as "O" (JCPDS card no 75–1621). The XRD of $Ni(OH)_2$ with peaks assigned for

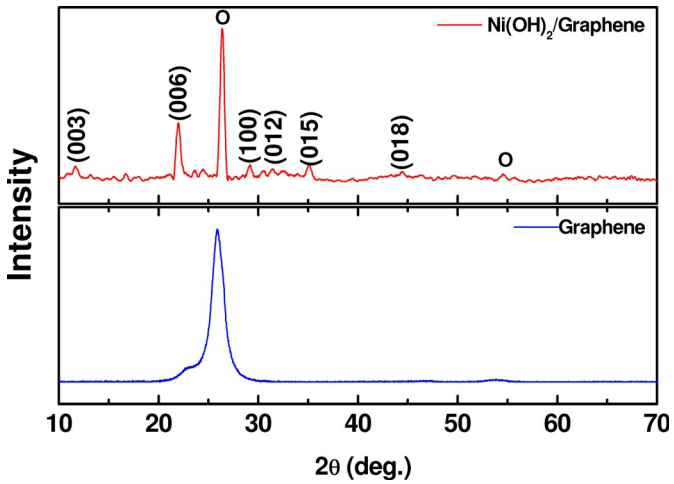

Fig. 2. The X-ray diffraction (XRD) patterns of $Ni(OH)_2$/3D-graphene and 3D-graphene.

(003), (006), (012), (015), (100) and (018) planes correspond to the hexagonal mixed phase of α- and β-$Ni(OH)_2$ (JCPDS card no. 38–0715) [21]. Also, the good crystallinity of the deposited films of $Ni(OH)_2$ materials can be assured by the high and sharper diffraction peaks. Thus solution growth method allows to form mixed (α and β) phase of $Ni(OH)_2$ on the graphene foam surface.

3.3 XPS Studies

To obtain more detailed information about elements and oxidation states of the as-prepared $Ni(OH)_2$/3D-graphene, X-ray photoelectron spectroscopy measurements were performed and the corresponding results are presented in Figure 3. The Survey of XPS data is shown in Figure 3a. The fitted spectra of C 1s for $Ni(OH)_2$/3D-graphene foam electrode are shown in Figure 3b. Figure 3b reveals that the peak centered at a binding energy of 284.68 eV represents C–C and C=C bonding and, along with shoulder peaks at 286.28 and 288.88 eV can typically be assigned for the C–O, COOH surface functional groups. The fitted spectrum for the O 1s region shown in Figure 3c reveals oxygen contributions in $Ni(OH)_2$/3D-graphene foam electrode. It is observed that the O 1s core level region is composed of a broad peak centered at 531.5 eV, which is associated with bound hydroxide groups (OH^-) and confirms the $Ni(OH)_2$ formation [22]. Thus, XPS studies support the formation of the Nickel hy-

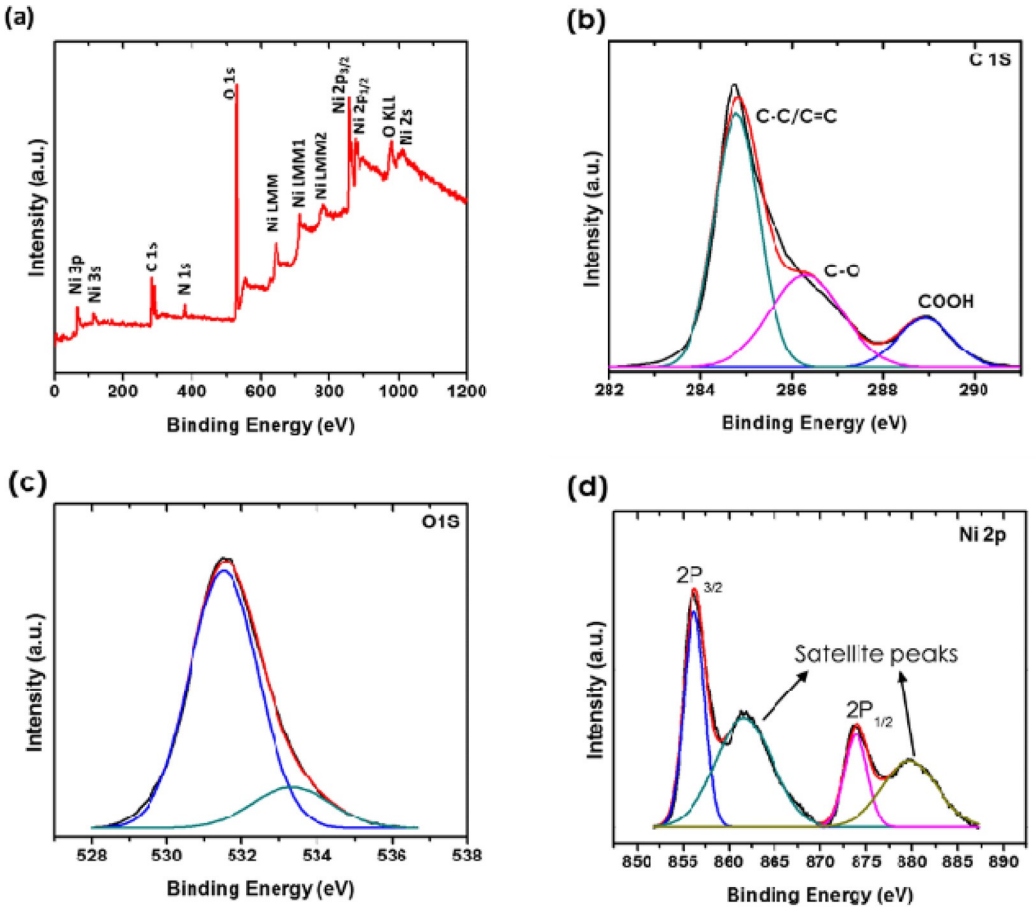

Fig. 3. X-ray photoelectron spectroscopy (XPS) measurements of (a) $Ni(OH)_2$/3D-graphene. Fitted XPS spectra of (b) C 1s, (c) O 1s, (d) Ni 2p for $Ni(OH)_2$/3D-graphene electrode.

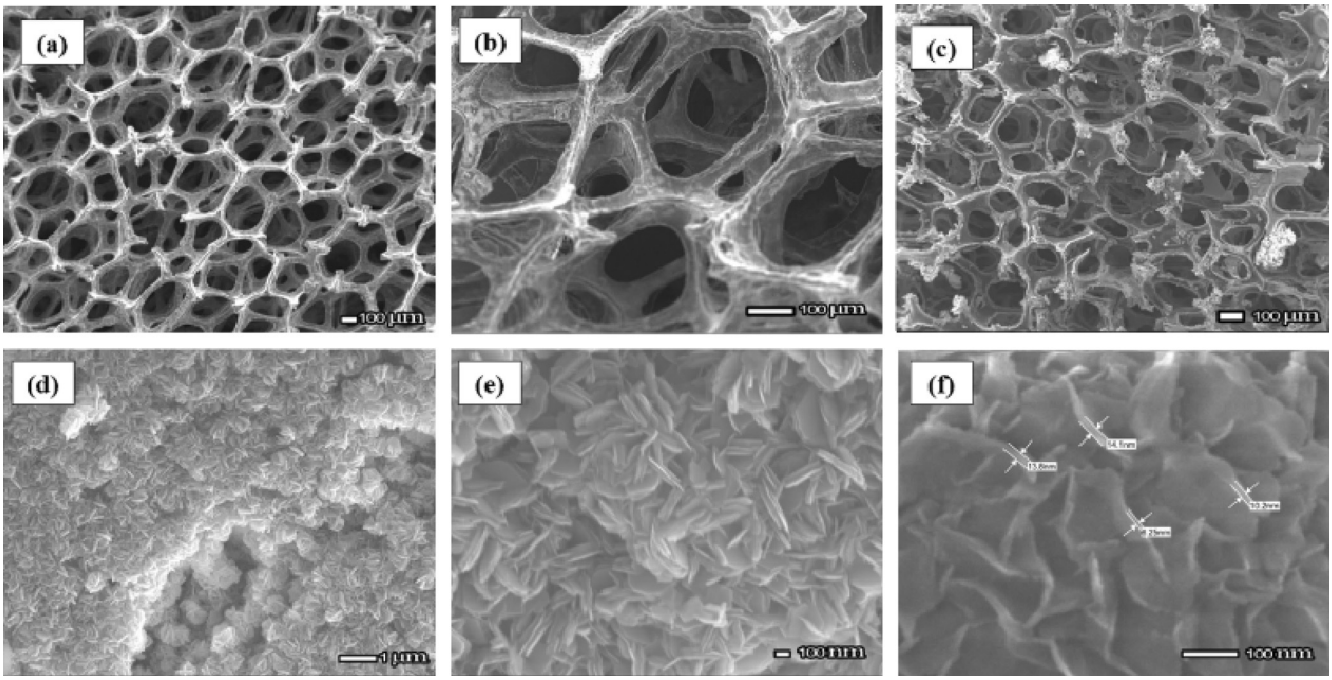

Fig. 4. scanning electron microscopy (SEM) for graphene is shown in (a) and (b). The twigs of graphene foam has been well covered by $Ni(OH)_2$ with overgrown particles at the edges (c). The higher magnification image of the surface morphology in (d, e) reveals that the graphene sheet is well-covered with a vertically aligned flake-like structure. The high magnification SEM image (f) demonstrates that these flakes are 5–10 µm in size with a width of 10–20 nm.

droxide phase on graphene foam. Figure 3d shows fitted spectra of Ni 2p for $Ni(OH)_2$/3D-graphene foam electrodes. The Ni 2p spectrum was best fitted by considering two spin-orbit doublets and two shakeup satellites. Two kinds of nickel species have been detected and assigned to species containing Ni^{2+} and Ni^{3+} ions [23]. Specifically, peaks at binding energies (BE) of 853.7 and 871.3 eV are ascribed to Ni2+, whereas the peaks at BE of 855.2 and 872.8 eV are assigned to Ni^{3+} [23]. The XPS result suggests that formation of Nickel hydroxide on graphene foam surface.

3.4 Surface Morphology

For the fabrication of 3D-graphene foam, graphene networks were grown by methane using CVD on Ni foam. The graphene foam maintains a 3D porous structure with a smooth and thin graphene skeleton after the exclusion of Ni. The morphology and structure of the graphene foam and $Ni(OH)_2$/3D-graphene composites were examined by FESEM, as shown in Figure 4. The graphene foam is a 3D porous structure with a smooth and thin graphene skeleton (Figure 4a and b). The Figure 4c shows that the twigs of graphene foam has been well covered by $Ni(OH)_2$ with overgrown particles at the edges. This overgrowth can be attributed to a nucleation and coalescence process. The higher magnification image of the surface morphology in Figures 4d,e reveals that the graphene sheet is well-covered with a vertically aligned flake-like structure. The high magnification SEM image (Figure 4f) demonstrates that these flakes are 5–10 µm in size with a width of 10–20 nm (Figure 4f). The SEM analysis confirms that the nanoflake structure of $Ni(OH)_2$ is formed on the graphene foam surface. Such flake-like morphology leads to be a high specific surface area, which provides the structural foundation for the high sensitivity.

3.5 Enzymless Glucose Detection by $Ni(OH)_2$/3D-Graphene Electrode

The $Ni(OH)_2$/3D-graphene electrode is advantageous for electrochemical applications, such as electrochemical sensing. $Ni(OH)_2$ is electrocatalytically active. N. Qiao et al. [8a] and recently Y. Jiang et al. [24] demonstrated the use of $Ni(OH)_2$ for sensitive, selective, and non-enzymatic detection of glucose. Prompted by this work, we sought to study the ability of the 3D-graphene/ $Ni(OH)_2$ electrode in non-enzymatic detection of glucose and increase the sensitivity. The Figure 5a presents the cyclic voltammetry (CV) curves over a voltage range from 0 to 0.6 V for the $Ni(OH)_2$/3D-graphene composite electrodes measured at different a scan rates from 20 to 100 mV s^{-1}. Evidently, the area surrounded by the CV curve is enhanced by the introduction of $Ni(OH)_2$ onto 3D-graphene foam as shown in Figure 5b. Increasing the scan rate leads to further augment of the CV curve and the redox peaks, indicating that the redox reactions of $Ni(OH)_2$ are rapid. It is noticeable that all of the CV curves exhibit two redox peaks arising from the quasi-reversible faradaic reaction in the alkaline electrolyte. The anodic peak

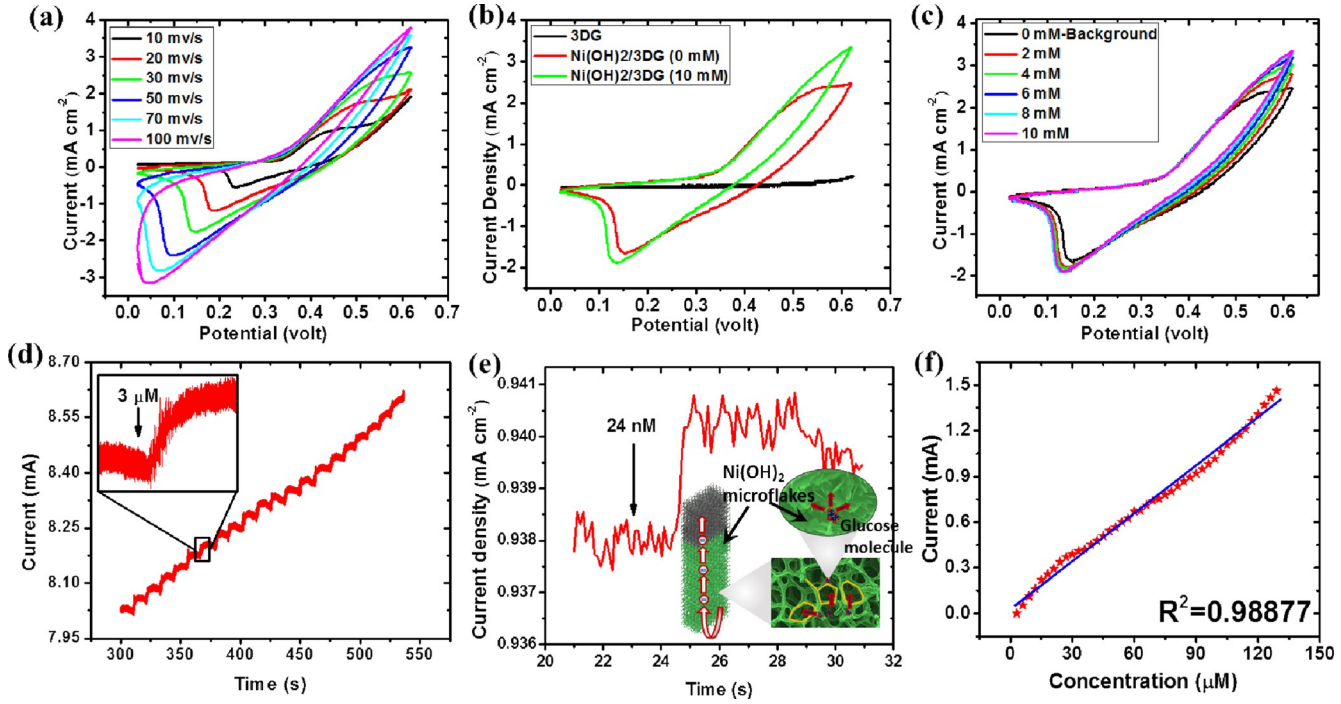

Fig. 5. Electrochemical performance of the $Ni(OH)_2$/3D-graphene electrodes measured in 1 M KOH solution. (a) CV curves of $Ni(OH)_2$/3D-graphene composite electrodes measured at a scan rate of 20 to 100 $mV\,s^{-1}$. (b) shows CV curves of 3D-graphene, Ni(OH)2/3D-graphene without glucose and in 10 mM of glucose. (c) CV curves in the presence of various concentrations of glucose (0 to 10 mM), at the scan rate of 20 $mV\,s^{-1}$. (d) The amperometric responses of the $Ni(OH)_2$/ 3D-graphene electrode to successive addition of glucose to increasing concentrations (e) demonstrate lower detection limit up to 24 nM and inset of the figure shows schematic charge transport of $Ni(OH)_2$/3D-grapheme electrode. The nanomolar dose response curve shows an amperometric current increase with increase in glucose concentration in scale. (f) Current response vs. glucose concentration.

(+*ve* current density) observed at 0.5 V (vs. Ag/AgCl) corresponds to an oxidation reaction $Ni(OH)_2$ to NiOOH, while the cathodic peak (−*ve* current density) which occurred around 0.12 V (vs. Ag/AgCl) indicates the reverse process, i.e., a reduction reaction. From Figure 5a, in the cyclic voltammograms $Ni(OH)_2$/3D-graphene electrodes, the redox reaction between $Ni(OH)_2$ and NiOOH can be expressed as follows [24]:

$$Ni(OH)_2 + OH^- \rightarrow NiOOH + H_2O + O^- \quad (4)$$

Introduction of glucose causes an obvious increase at the oxidation peak current as shown in Figure 5c. To avoid changing the pH of KOH, the glucose solution was made in 1 M of PBS as buffer. With increase of glucose concentration, the oxidation current at positive potential also increased, while the reduction currents at negative potential is almost constant. It is well known that the $Ni(OH)_2$/3D-graphene electrode oxidation of glucose will consume glucose and produce glucolactone. The glucose sensing by $Ni(OH)_2$/3D-graphene electrodes can be expressed by following reaction [24].

$$Ni(OH)_2 + OH^- \rightarrow NiOOH + H_2O + e^- \quad (5)$$

$$NiOOH + \text{glucose} \rightarrow Ni(OH)_2 + \text{gluconolactone} \quad (6)$$

Holding at the oxidation potential of peak (0.45 V), the amperometric responses of the $Ni(OH)_2$/3D-graphene composite electrode to successive addition of glucose to increasing concentrations were measured in 3 micromolar (Figure 5d). The amperometric current response found to be 10.47 $\mu A\,cm^{-2}$ for 3 μM glucose addition. The dose response curve shows an amperometric current increase by adding glucose. The linearity of the graph attributed to the good stability with stable sensing of $Ni(OH)_2$/3D-graphene electrode at low concentration. Amperometric response of $Ni(OH)_2$/3D-graphene is almost linear ($R^2 = 0.98877$) (see Figure 5f). To obtain the detection limit of $Ni(OH)_2$/3D-graphene electrode, the electrode tested for 24 nanomolar glucose sensing as shown in Figure 5e. To attain this value we add certain concentration of glucose each time, while measuring the current density in a constant potential of 0.45 volt. We decrease glucose concentration in several steps to obtain the minimum concentration that $Ni(OH)_2$/3D-graphene electrode can sense. The lower concentration of glucose (less than 24 nM) didn't shows significant linear range. Consequently we reported 24 nM as lowest detection limit for $Ni(OH)_2$/3D-graphene. The sensitivity of 3.49 $mA\,mM^{-1}\,cm^{-2}$ and significant lower detection limit up to 24 nM is obtained.

The stability test was carried out for over 100 cycles for $Ni(OH)_2$/3D-graphene electrode at each 3 μM concentra-

Table 1. A rough comparison of the obtained sensitivity at particular glucose concentration, linear range, low detection limit, with some recent reports.

Glucose sensor	Detection limit (μM)	Linear range (μM)	Sensitivity ($mA\,mM^{-1}\,cm^{-2}$)	Date and reference
$Ni(OH)_2$/3D-graphene	0.024	0.024–1200	3.49	Present work
$Ni(OH)_2$/3D-graphene	0.34	1–1170	2.65	[19]
CoO/3D-graphene	0.025	Up to 300	3.390	[7b]
PI/CNT–$Ni(OH)_2$ nanospheres	0.36	0.1–800	2.0715	[24]
CoOOH nanosheets	10.6	10–500	0.967	[28]
NiCFP electrode	1	2×10^{-6}–2.5×10^{-3}	0.4204	[29]
$Ni(OH)_2$ CILE	6	5×10^{-5}–23×10^{-3}	0.202	[30]
(Ni-Co)$(OH)_2$	25	25–3700	0.12245	[10]
PtPb/MWCNT	1.8	Up to 11000	0.0178	[31]
rGO-$Ni(OH)_2$/GCE	0.6	2–3100	0.01143	[32]

tion of glucose. The SEM images of $Ni(OH)_2$/3D-graphene electrode for before sensing and after 100 cycles were carried out and shown figure S3 (See supporting information). The SEM images reveals that, the flake like morphology of $Ni(OH)_2$ is changed into some cluster like morphology after 100 cycles of sensing. This result suggests that, the $Ni(OH)_2$/3D-graphene electrode is quite stable after 100 cycles of sensing.

The EIS is powerful, non-destructive and useful technique, which is usually used for characterization studies. However EIS was used for quantitative determination of glucose [25]. In this work, the EIS study of the modified electrodes was performed in a 1 M KOH solution from 0 up to 2.0 mM Glucose concentration. Instead of Nyquist plot of EIS, Figure S2a (see Supporting Information) reveals the relation of real impedance and frequency. According to Equation 6, increasing the concentration glucose, formed more $Ni(OH)_2$ lead to more electrons(e^-) based on Equation 5. Thus, real impedance was decreased after adding glucose due to increasing the amount of electrons in solution.

The reproducibility of the sensor's measurement of glucose was also experienced with 15 different concentrations of glucose in nano-, micro- and milli-molar scale (see Table S1 in Supporting Information). The calculated *RSD* values of the glucose were almost below 9%, which indicates that the repeatability of the biosensors is practically acceptable [26].

To obtain the best time duration for chemical bath deposition (CBD) 3 samples were prepared which are 1, 2 and 3 for 6, 8 and 10 hours respectively. Then real electrochemical catalytic surface area of the working electrode is estimated from the Randles–Sevcik equation [27]. Since the effective surface area (A) is proportional to $I_p v^{-1/2}$, cyclic voltammograms of the electrodes were measured in a 3 M KCl solution containing 10 mM of $K_3Fe(CN)_6$ (potassium ferricyanide) at a variety of scan rates (see Figure S2b Supporting Information). Figure S3c shows that the relationships between the peak current (I_p) and the square root of the potential scan rate ($v^{1/2}$) are linear for all electrodes for all of samples. Table S2 (see Supporting Information) shows that effective surface area improved as the duration of CBD increased.

In real samples, selectivity is another main factor to evaluate the performance of the $Ni(OH)_2$/3DGF electrode for nonenzymatic glucose detection. The oxidizable compounds such as ascorbic acid (AA), uric acid (UA) and other carbohydrates such as fructose and sucrose often interfere with the analysis of glucose. In this regard, reducible of oxidizable of $Ni(OH)_2$ at a constant potential of 0.45 V that is applied in this report for amperometric studying is well studied in previous reports [8a]. B. Zhan et al. [19] indicated that $Ni(OH)_2$/3DGF could be used for detection of glucose with negligible interference from dopamine, lactose, D-fructose, L-ascorbic acid and urea.

A rough comparison of the obtained sensitivity at particular glucose concentration, linear range, low detection limit, with some recent reports, is given in Table 1. Table 1 depicts that the sensitivity at lower glucose concentration (24 nM) obtained in the present work surpasses previous literature values reported for Ni/NiO-graphene, CoO/3D-graphene, CNT-$Ni(OH)_2$ and even $Ni(OH)_2$/3D-graphene with different preparing treatment. The obtained maximum sensitivity at lower glucose concentration is higher than that reported for pure $Ni(OH)_2$ and its composite with 2D/3D-graphene and CNT. The 3D-grapheme foam provides a highly conductive network to enhance the electron transport to the $Ni(OH)_2$, the porous $Ni(OH)_2$ microflake structure shortens ion diffusion paths and facilitates migration of Glucose ions at a large current density (schematic of charge transport mechanism shown in inset of Figure 5e), and direct growth by solution growth method avoids the addition of binder and a metal-based current collector which not only hamper the charge transport rate, but also increases the total mass of the electrode. As well as, the $Ni(OH)_2$/3D-graphene electrode offers many advantageous than other conventional glucose sensing electrodes such as light weight, 3D porous structure with good conducting structure. Such wide range of benefits including high sensitivity, low detection limit with unique structure of $Ni(OH)_2$/3D-graphene electrode underlines its potential industrial application in glucose sensors.

4 Conclusions

Present work demonstrates that chemically grown Ni(OH)2 is good candidate for glucose detection along with 3D-graphene with its assistances as a free standing electrode. 3D-graphene with its pore structures, increases the surface area and offers more deposites for $Ni(OH)_2$ nanoflakes on it. Consequently, the high surface area, good conducting structure of $Ni(OH)_2$/3D-graphene electrode sensitize glucose very efficiently. The unique structure of $Ni(OH)_2$/3D-graphene present lower detection limit up to 24 nM with good linearity. The high sensitivity, good linearity and low detection limit establishes $Ni(OH)_2$/3D-graphene electrode as a exceptional enzymless glucose sensor.

Acknowledgements

This work was partially supported by the *Yonsei University* Research Fund of 2013, the Pioneer Research Center Program (2010-0019313), the Priority Research Centers Program (2009-0093823), the Basic Science Research Program (2014110553) through the *National Research Foundation* (*NRF*) of Korea funded by the *Ministry of Science, ICT & Future Planning* and *Korea Electric Power Corporation Research Institute* through *Korea Electrical Engineering & Science Research Institute* (Grant Number: R14XA02-2).

References

[1] a) S. M. U. Ali, O. Nur, M. Willander, B. Danielsson, *Sens. Actuators B, Chem.* **2010**, *145*, 869–874; b) R. Nenkova, D. Ivanova, J. Vladimirova, T. Godjevargova, *Sens. Actuators B Chem.* **2010**, *148*, 59–65; c) Q. Sheng, Y. Shen, H. Zhang, J. Zheng, *Electrochim. Acta* **2008**, *53*, 4687–4692.
[2] S. Park, H. Boo, T. D. Chung, *Anal. Chim. Acta* **2006**, *556*, 46–57.
[3] a) C.-H. Xue, R.-J. Zhou, M.-M. Shi, G. Wu, X.-B. Zhang, M. Wang, H.-Z. Chen, *J. Electroanal. Chem.* **2010**, *642*, 92–97; b) X. Kang, J. Wang, H. Wu, I. A. Aksay, J. Liu, Y. Lin, *Biosens. Bioelectron.* **2009**, *25*, 901–905.
[4] C. Li, Y. Su, S. Zhang, X. Lv, H. Xia, Y. Wang, *Biosens. Bioelectron.* **2010**, *26*, 903–907.
[5] F. Cao, S. Guo, H. Ma, D. Shan, S. Yang, J. Gong, *Biosens. Bioelectron.* **2011**, *26*, 2756–2760.
[6] J. Chen, W.-D. Zhang, J.-S. Ye, *Electrochem. Commun.* **2008**, *10*, 1268–1271.
[7] a) Y. Ding, Y. Wang, L. Su, M. Bellagamba, H. Zhang, Y. Lei, *Biosens. Bioelectron.* **2010**, *26*, 542–548; b) X.-C. Dong, H. Xu, X.-W. Wang, Y.-X. Huang, M. B. Chan-Park, H. Zhang, L.-H. Wang, W. Huang, P. Chen, *ACS nano* **2012**, *6*, 3206–3213.
[8] a) N. Qiao, J. Zheng, *Microchim. Acta* **2012**, *177*, 103–109; b) Q. Yi, J. Zhang, W. Huang, X. Liu, *Catalysis Commun.* **2007**, *8*, 1017–1022.
[9] L. Cui, H. Yin, J. Dong, H. Fan, T. Liu, P. Ju, S. Ai, *Biosens. Bioelectron.* **2011**, *26*, 3278–3283.
[10] C.-H. Lien, J.-C. Chen, C.-C. Hu, D. S.-H. Wong, *J. Taiwan Inst. Chem. Eng.* **2014**, *45*, 846–851.
[11] a) Y. Mu, D. Jia, Y. He, Y. Miao, H.-L. Wu, *Biosens. Bioelectron.* **2011**, *26*, 2948–2952; b) M. Shamsipur, M. Najafi, M.-R. M. Hosseini, *Bioelectrochemistry* **2010**, *77*, 120–124.
[12] a) K. E. Toghill, L. Xiao, M. A. Phillips, R. G. Compton, *Sens. Actuators B, Chem.* **2010**, *147*, 642–652; b) A. Safavi, N. Maleki, E. Farjami, *Biosens. Bioelectron.* **2009**, *24*, 1655–1660.
[13] H. Park, H. S. Yoon, U. Patil, R. Anoop, J. Lee, J. Lim, W. Lee, S. C. Jun, *Biosens. Bioelectron.* **2014**, *54*, 141–145.
[14] a) A. A. Balandin, S. Ghosh, W. Bao, I. Calizo, D. Teweldebrhan, F. Miao, C. N. Lau, *Nano Lett.* **2008**, *8*, 902–907; b) K. Kim, H. J. Park, B.-C. Woo, K. J. Kim, G. T. Kim, W. S. Yun, *Nano Lett.* **2008**, *8*, 3092–3096.
[15] A. K. Geim, K. S. Novoselov, *Nature Mater.* **2007**, *6*, 183–191.
[16] C. Shan, H. Yang, D. Han, Q. Zhang, A. Ivaska, L. Niu, *Biosens. Bioelectron.* **2010**, *25*, 1070–1074.
[17] X. Dong, S. Argekar, P. Wang, D. W. Schaefer, *ACS Appl. Mater. Interf.* **2011**, *3*, 4206–4214.
[18] Z. Chen, W. Ren, L. Gao, B. Liu, S. Pei, H.-M. Cheng, *Nature Mater.* **2011**, *10*, 424–428.
[19] B. Zhan, C. Liu, H. Chen, H. Shi, L. Wang, P. Chen, W. Huang, X. Dong, *Nanoscale* **2014**, *6*, 7424–7429.
[20] U. M. Patil, J. S. Sohn, S. B. Kulkarni, S. C. Lee, H. G. Park, K. V. Gurav, J. Kim, S. C. Jun, *ACS Appl. Mater. Interf.* **2014**, *6*, 2450–2458.
[21] a) U. Patil, K. Gurav, V. Fulari, C. Lokhande, O. S. Joo, *J. Power Sources* **2009**, *188*, 338–342; b) Y.-X. Wang, Z.-A. Hu, H.-Y. Wu, *Mater. Chem. Phys.* **2011**, *126*, 580–583.
[22] a) D. Yang, A. Velamakanni, G. Bozoklu, S. Park, M. Stoller, R. D. Piner, S. Stankovich, I. Jung, D. A. Field, C. A. Ventrice, *Carbon* **2009**, *47*, 145–152; b) J.-C. Dupin, D. Gonbeau, P. Vinatier, A. Levasseur, *Phys. Chem. Chem. Phys.* **2000**, *2*, 1319–1324.
[23] A. P. Grosvenor, M. C. Biesinger, R. S. C. Smart, N. S. McIntyre, *Surf. Science* **2006**, *600*, 1771–1779.
[24] Y. Jiang, S. Yu, J. Li, L. Jia, C. Wang, *Carbon* **2013**, *63*, 367–375.
[25] R. K. Shervedani, A. H. Mehrjardi, N. Zamiri, *Bioelectrochemistry* **2006**, *69*, 201–208.
[26] a) G. Li, J. Liao, G. Hu, N. Ma, P. Wu, *Biosens. Bioelectron.* **2005**, *20*, 2140–2144; b) M. J. Song, J. H. Kim, S. K. Lee, D. S. Lim, S. W. Hwang, D. Whang, *Electroanalysis* **2011**, *23*, 2408–2414.
[27] A. J. Bard, L. R. Faulkner, *Electrochemical Methods: Fundamentals and Applications*, Vol. 2, Wiley, New York, **1980**.
[28] H. Zeng, C. Gao, Y. Wang, P. C. Watts, H. Kong, X. Cui, D. Yan, *Polymer* **2006**, *47*, 113–122.
[29] Y. Liu, H. Teng, H. Hou, T. You, *Biosens. Bioelectron.* **2009**, *24*, 3329–3334.
[30] J. W. Lee, J. M. Ko, J.-D. Kim, *J. Phys. Chem. C* **2011**, *115*, 19445–19454.
[31] H.-F. Cui, J.-S. Ye, W.-D. Zhang, C.-M. Li, J. H. Luong, F.-S. Sheu, *Anal. Chim. Acta* **2007**, *594*, 175–183.
[32] Y. Zhang, F. Xu, Y. Sun, Y. Shi, Z. Wen, Z. Li, *J. Mater. Chem.* **2011**, *21*, 16949–16954.

Received: January 6, 2015
Accepted: March 23, 2015
Published online: July 14, 2015

